ELSEVIER

Contents lists available at ScienceDirect

# Spectrochimica Acta Part B: Atomic Spectroscopy

journal homepage: www.elsevier.com/locate/sab





# Spectroscopic signatures and oxidation characteristics of nanosecond laser-induced cerium plasmas

Emily H. Kwapis <sup>a,\*</sup>, Eliel Villa-Aleman <sup>b</sup>, Kyle C. Hartig <sup>a</sup>

- a Nuclear Engineering Program, Department of Materials Science and Engineering, University of Florida, Gainesyille, FL 32611, USA
- <sup>b</sup> Savannah River National Laboratory, Aiken, SC 29808, USA

#### ARTICLE INFO

Keywords:
Cerium
Laser ablation
Laser-induced breakdown spectroscopy
Plasma chemistry
Oxidation

#### ABSTRACT

Improving technologies related to the wide area environmental sampling of nuclear materials supports the nuclear nonproliferation mission of preventing the proliferation of nuclear weapons by monitoring nuclear weapons tests and detecting undeclared nuclear fuel cycle activities. Standoff, laser-based detection techniques such as laser-induced breakdown spectroscopy have the potential to offer robust, field-deployable methods that provide rapid element-specific and phase identifiable measurements over a wide range of materials. This work aims to elucidate the effects of atmospheric conditions and oxidation reactions on the highly complex and transient spectroscopic signatures of laser-induced plutonium surrogate plasmas. Time-resolved spectra of nanosecond laser ablation cerium plasmas were measured using laser-induced breakdown spectroscopy in a range of atmospheres containing low to high concentrations of oxygen. The growth of strong CeO molecular emission bands was observed in the visible spectrum, where it was shown that the persistence of CeO is reduced from around 60 μs to 50 μs in oxygen rich atmospheric environments. To further investigate the growth and depletion of CeO in the laser-produced plasma, ratios of CeO-to-Ce emission were generated using integrated intensities corresponding to the Q-branch of the CeO D<sub>1</sub>-X<sub>1</sub> transitions and numerous strong atomic Ce peaks. It was determined that the fastest rate of formation of CeO in argon occurred for moderate oxygen mass fractions between 0.10 and 0.15 while the ratios were reduced at higher oxygen mass fractions (i.e.,  $Y_{O_2} = 0.20$ ) due to competing oxidation reactions and lower plasma temperatures.

# 1. Introduction

The ability to detect nuclear materials in the environment is essential to the nuclear nonproliferation mission of preventing the spread of nuclear weapons and responding to nuclear explosion events. Laser ablation coupled with optical spectroscopy provides the capability to perform rapid spectrochemical analyses with no sample preparation at standoff distances in-the-field [1]. Through the process of laser ablation (LA), a high-powered pulsed laser pulse is used to vaporize a small mass ( $\approx$ pg-ng) of a solid sample to produce a highly luminous micro-plasma, which is typically characterized by initial temperatures and electron densities of  $\approx$ 2 eV and  $10^{21}$  cm $^{-3}$ [2–4]. Laser-induced plasmas (LIP), or laser-produced plasmas (LPP), are highly transient and within less than a microsecond quickly decay to temperatures less than 1 eV and densities in the range of  $10^{14}$ – $10^{18}$  cm $^{-3}$ [5,6]. It is during this regime that optical spectroscopy techniques are applied to identify and characterize the vapor-phase atoms, ions, and molecules present in the plasma that

originate from the ablated sample and incorporated material from the surrounding environment. The ions and neutral atoms are typically observed to dominate the composition of the plasma at early times (<1  $\mu$ s) while molecules form at later times as a result of the lower plasma temperatures and mixing of the plasma with the environment [7]. The thermodynamics of these chemical reactions play an important role in driving the plasma temperature. Additionally, chemical reactions may also considerably impact particle formation and debris distribution in post-detonation fireballs, where laser plasmas have repeatedly been used as surrogates for chemical detonations of energetic materials to study the physical and chemical processes governing the growth and evolution of the detonation [7–10]. Laser-produced plasmas have also been used as surrogates for uranium nuclear fireballs to study the physical and chemical processes of nuclear explosions [11–16].

Experimental research on these nuclear fireball surrogates has focused largely on the high-temperature gas-phase oxidation chemistry of uranium LPPs in the past decade, where a single uranium monoxide

E-mail address: ekwapis@ufl.edu (E.H. Kwapis).

<sup>\*</sup> Corresponding author.

(UO) band situated around 593.55 nm is targeted to explain the complex chemical reactions driving the evolution of the laser-produced plasma plume [17-21]. It has been shown repeatedly that the temporal evolution of uranium plasmas is sensitive to the presence of reactive species (e.g., oxygen) in the environment, where the associated chemical reactions are known to strongly depend on temperature. The formation of UO is believed to be favored between  $\approx 3,000-6,000$  K [22]. During the formation of UO, atomic uranium is consumed resulting in a measured decrease in the persistence, or lifetime, of spectral signals for atomic uranium. This behavior has been demonstrated consistently for uranium plasmas using inert environments compared to atmospheres containing oxygen [19,21]. Additionally, a reduction in the persistence of UO has been reported in oxygen-rich environments, such as for standard atmospheric conditions in air [20,22]. This reduction in the monoxide persistence is believed to be due to the depletion of UO during the formation of polyatomic uranium oxides (UxOv), although resolved molecular signatures for the higher uranium oxides are not typically studied alongside UO and specific assignments for these oxide phases are frequently left undetermined [14,17,21,22]. Within the last few years, there has been an effort to extend this work to select polyatomic uranium oxides (UO<sub>2</sub>, UO<sub>3</sub>, U<sub>3</sub>O<sub>8</sub>, etc.) as well as to study uranium plasma chemistry with silicon to provide further insights into nuclear fallout formation [16,23-26]. Yet, while a significant effort continues to be focused on the high-temperature gas-phase combustion chemistry of uranium, important investigations into debris formation pathways of the other actinides are largely untouched. The detection of both uranium and plutonium in the environment is essential to prevent the proliferation nuclear weapons and to characterize post-detonation nuclear environments. However, equivalent research on the high-temperature gasphase chemistry of plutonium LPPs is severely lacking in the literature despite marked differences in chemistry between the elements. To address these current knowledge gaps, this work aims to explain the physical and chemical behavior of plutonium plasmas using laser spectroscopy techniques.

Plutonium is known to be characterized by a very complex electronic structure and chemical behavior encompassing a high number of oxidation states, multiple allotropic forms, and high sensitivity to external influences, such as pressure changes and alloying [27,28]. Atomic emission lines for <sup>239</sup>Pu and <sup>240</sup>Pu are known and published in various reports [29,30]. Laser-induced breakdown spectroscopy (LIBS) experiments leveraging these atomic emission lines have historically focused on identifying main components and impurities in mixed actinide oxide fuel pellet surrogates [31,32], and have also been applied to measure isotope shifts [33]. Other spectroscopy techniques such as photoelectron spectroscopy (PES) have been applied to study the surface oxidation of  $\alpha$ - and  $\delta$ -phase plutonium metals [34,35]. M.T. Butterfield et al. (Ref. 35) showed that in oxygen deficient atmospheres that the sesquioxide phase is favored, while otherwise the dioxide phase is favored. As for investigations into the gas-phase oxidation chemistry of plutonium at high temperatures (>2,000 K), the literature is extremely limited. To the best of the authors' knowledge, there has been only a single attempt at studying the plasma chemistry of plutonium LPPs, where LIBS was performed with ns-LA on a plutonium metal sample and potential plutonium oxide bands were visually identified based on the temporal behavior and shape of the emission signatures [36]. However, specific Pu<sub>x</sub>O<sub>y</sub> transitions could not be determined due to the lack of any database containing molecular plutonium oxide bands in the visible spectrum. Kaledin and Heaven et al. have conducted a significant effort towards labeling the ro-vibrational absorption, fluorescence, and emission signatures of UO and CeO using high-resolution laser spectroscopy, yet have not presently extended this work to plutonium [37-44]. Therefore, an alternative approach must be taken to study the complicated plutonium-oxygen system to provide insights into debris formation pathways for plutonium nuclear fireballs.

Historically, surrogates have frequently been used to investigate plutonium systems, where cerium is chosen due to similarities in electronic, physical, chemical, and thermodynamic properties [45–51]. Both elements are characterized by complex, yet comparable chemistry and surface oxidation pathways due to the degree of localization of their f-electrons [52-55]. Fundamental optical properties of cerium are known and have been studied for a range of applications including thin film synthesis through pulsed laser deposition [56], semiconductor device design [57,58], nuclear fuel materials analysis [59–61], and the detection of cerium in mixed samples [60,62–64]. Databases containing optical transitions and associated spectroscopic constants for neutral and ionized atomic cerium are available [65,66]. In contrast to plutonium, molecular constants for cerium oxide transitions have been measured and are provided in various publications in the literature [40-44]. This availability of labeled CeO transitions enables investigations into the vapor-phase oxidation chemistry of cerium plasmas; yet few studies regarding the influences of environmental factors (e.g., pressure, oxygen concentration) on the optical spectrum of cerium have been conducted. Of these limited studies, a Langmuir probe has been used to measure ion and electron densities in a cerium plasma at low bulk pressures (<0.133 Pa), where the ion density of cerium and oxygen was reported to decrease as oxygen partial pressures increased indicating the formation of cerium oxides [56].

Altogether, the work presented in this paper encompasses the early gas-phase oxidation chemistry of cerium LPPs as a chemical surrogate for the plutonium—oxygen system. While the discrete energies of the atomic and molecular signatures between cerium and plutonium will differ, the chemical and thermodynamic properties of the cerium-oxygen system are expected to be characterized by analogous behaviors to that of the plutonium—oxygen system. To investigate these behaviors and the temporal evolution of oxide growth in cerium LPPs, nanosecond-LA will be implemented with laser-induced breakdown spectroscopy to analyze the progression of atomic and molecular cerium signatures over time.

# 2. Experimental setup and methods

LIBS was applied to measure spectroscopic signatures for atomic and molecular cerium species to study the high-temperature gas-phase oxidation chemistry of cerium LPPs. Experiments were performed within a controlled environment using a custom vacuum chamber, where measurements were collected at atmospheric pressure in air as well as in an inert argon atmosphere at a bulk pressure of 13.3 kPa. To elucidate the effect of chemical reactions with oxygen on the spatiotemporal evolution and spectroscopic signatures of cerium plasmas, various mass fractions of oxygen ranging from 0.01 and 0.20 are introduced to the inert argon gas to simulate oxygen deficient and oxygen rich atmospheric conditions.

LIBS was performed using the fundamental wavelength (1064 nm) of a Nd:YAG laser with a pulse width of  $\approx$ 6 ns and beam energy of 60.5  $\pm$ 0.5 mJ to ablate a cerium metal sputtering target (MSE Supplies, 99.9% purity). The laser beam was focused on the target using a 100 mm focal length plano-convex convex lens and spot size of  $\approx$ 400  $\mu m$  in diameter. Cleaning shots were applied prior to collecting emission spectra to remove the thick oxide layer that coats the cerium metal sample. However, influences due to oxygen entrained in this oxide layer could not be completely eliminated and the consequential plasma oxidation chemistry was observed to be comparable to oxygen deficient environments (i.e.,  $Y_{O_2} = 0.01$ ). The light emitted from the cerium plasma was collected using a 100 mm focal length plano-convex lens paired with a second 50 mm focal length plano-convex lens oriented approximately  $30^{\circ}$  to the target surface. This collection system was then coupled to a  $200 \, \mu m$  optical fiber and directed into a  $0.5 \, m$  focal length triple grating spectrograph (Princeton Instruments Acton SpectraPro SP-2500) and intensified EMCCD camera (Princeton Instruments PI-MAX4 emICCD). The spectrometer was calibrated at a slit width of 30 µm and 2400 g/mm grating using a mercury lamp, where instrumental broadening was measured to be 47.5 pm FWHM at 435.83 nm. For measurements

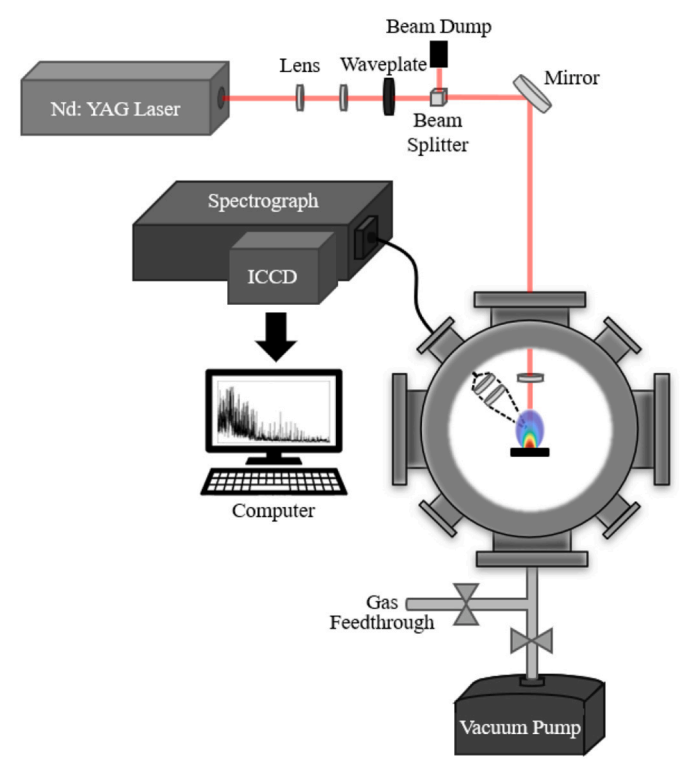


Fig. 1. Experimental setup for laser-induced breakdown spectroscopy of a cerium metal sample using nanosecond laser ablation.

recorded at wavelengths greater than 700 nm, a lower resolution 1200 g/mm grating was used. The experimental setup for this work is shown in Fig. 1.

#### 3. Results and discussion

# 3.1. Elucidating CeO molecular emission signatures

Spectroscopic signatures of atomic cerium are characterized by a complex spectrum consisting of more than 30,000 emission lines resulting from more than 1,000 energy levels [67–70]. This yields a very crowded spectrum, which is complicated further by the formation of molecular species in oxidizing environments. Cerium readily reacts with oxygen to form cerium oxides such as cerium monoxide (CeO), cerium dioxide (CeO2), and cerium sesquioxide (Ce2O3), where CeO is characterized by ro-vibrational emission lines that fall within the visible spectrum and overlap with atomic Ce transitions. To study the oxidation chemistry and formation of CeO in laser-produced cerium plasmas, strong CeO bands that fall within the visible spectrum must first be determined and CeO features that do not overlap significantly with atomic emission lines must be identified. To address this, laser-induced breakdown spectroscopy was performed on a cerium metal target at atmospheric pressure in air. Molecular transitions were then visually identified based on their characteristic shape and labeled using available reports on CeO transitions in the literature.

During this process, several strong CeO emission bands were identified in the spectra including the  $D_1\text{-}X_1$ ,  $D_3\text{-}X_3$ ,  $B_2\text{-}X_2$ , and  $[14.7]_3\text{-}W_2$  transitions (see Fig. 2) using references [40–42]. Naming conventions used here follow those given by Kaledin and Heaven et al. in their numerous laser spectroscopy publications [37,38,41], where [14.7]\_3 refers to an energy state with a vibronic term value of  $\approx\!14700~\text{cm}^{-1}$  and quantum number  $\Omega=3$ . Additional CeO bands beyond those labeled in this work are present in the visible spectrum, yet were observed to be obscured by background and line broadening and were not well resolved. In contrast, the  $D_1\text{-}X_1$  transition is clearly detectable, where each individual branch (P, Q, and R) contained within the band is identifiable. More importantly, the head of the Q-branch does not

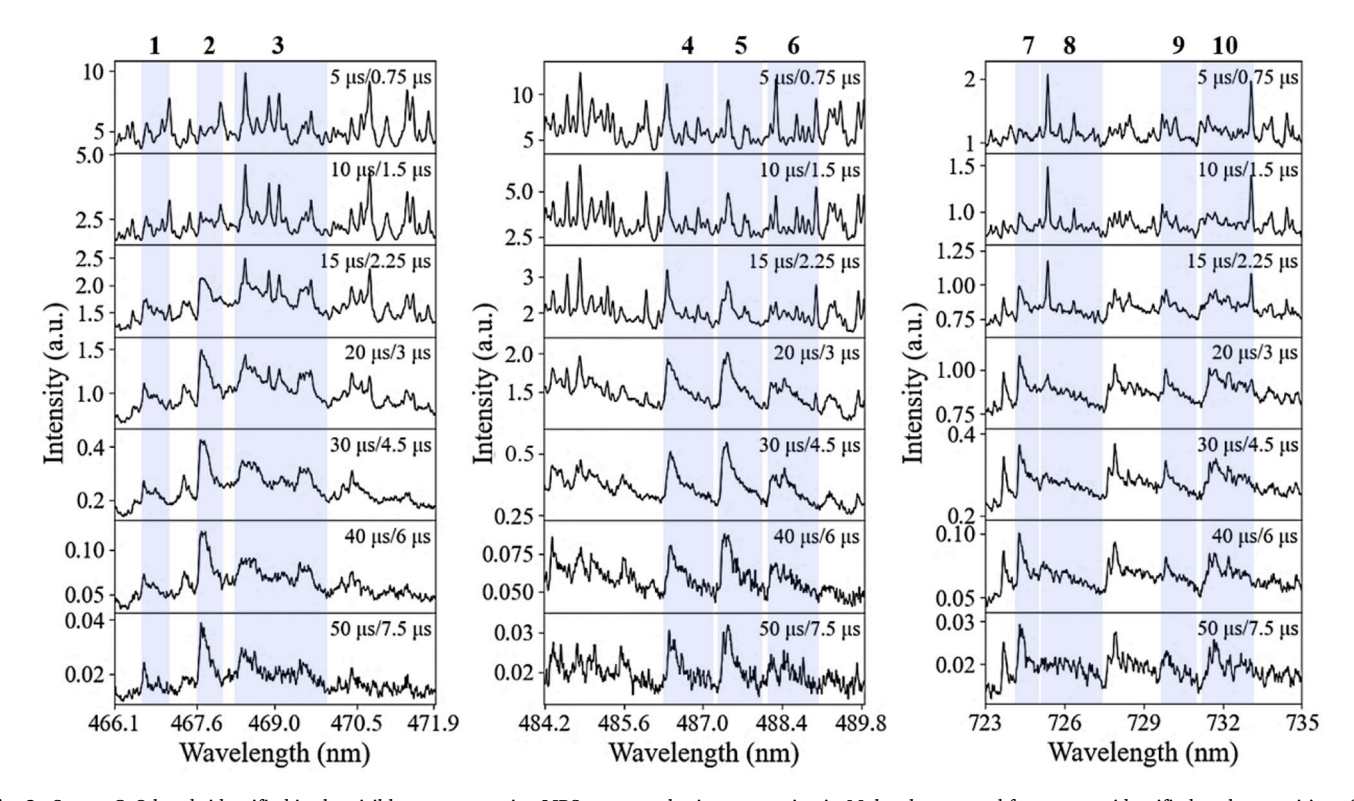


Fig. 2. Strong CeO bands identified in the visible spectrum using LIBS at atmospheric pressure in air. Molecular spectral features are identified as the transitions (1)  $D_1$ - $X_1$  0–0 R-branch, (2)  $D_1$ - $X_1$  0–0 Q-branch, (3)  $D_1$ - $X_1$  0–0 P-branch, (4)  $D_3$ - $X_3$  0–0 R-branch, (5)  $D_3$ - $X_3$  0–0 Q/P-branch, (6)  $D_3$ - $X_3$  1–1 (hot band), (7)  $B_2$ - $X_2$  0–0 R/Q-branch and [14.7]<sub>3</sub>- $W_2$  0–0 R-branch, (8) [14.7]<sub>3</sub>- $W_2$  0–0 Q-branch, (9)  $B_2$ - $X_2$  1–1 P-branch (hot band), and (10)  $B_2$ - $X_2$  2–2 R-branch (hot band), where branch assignments correspond to the head-forming branch. Times provided represent the delay times and gate widths of the measurements.

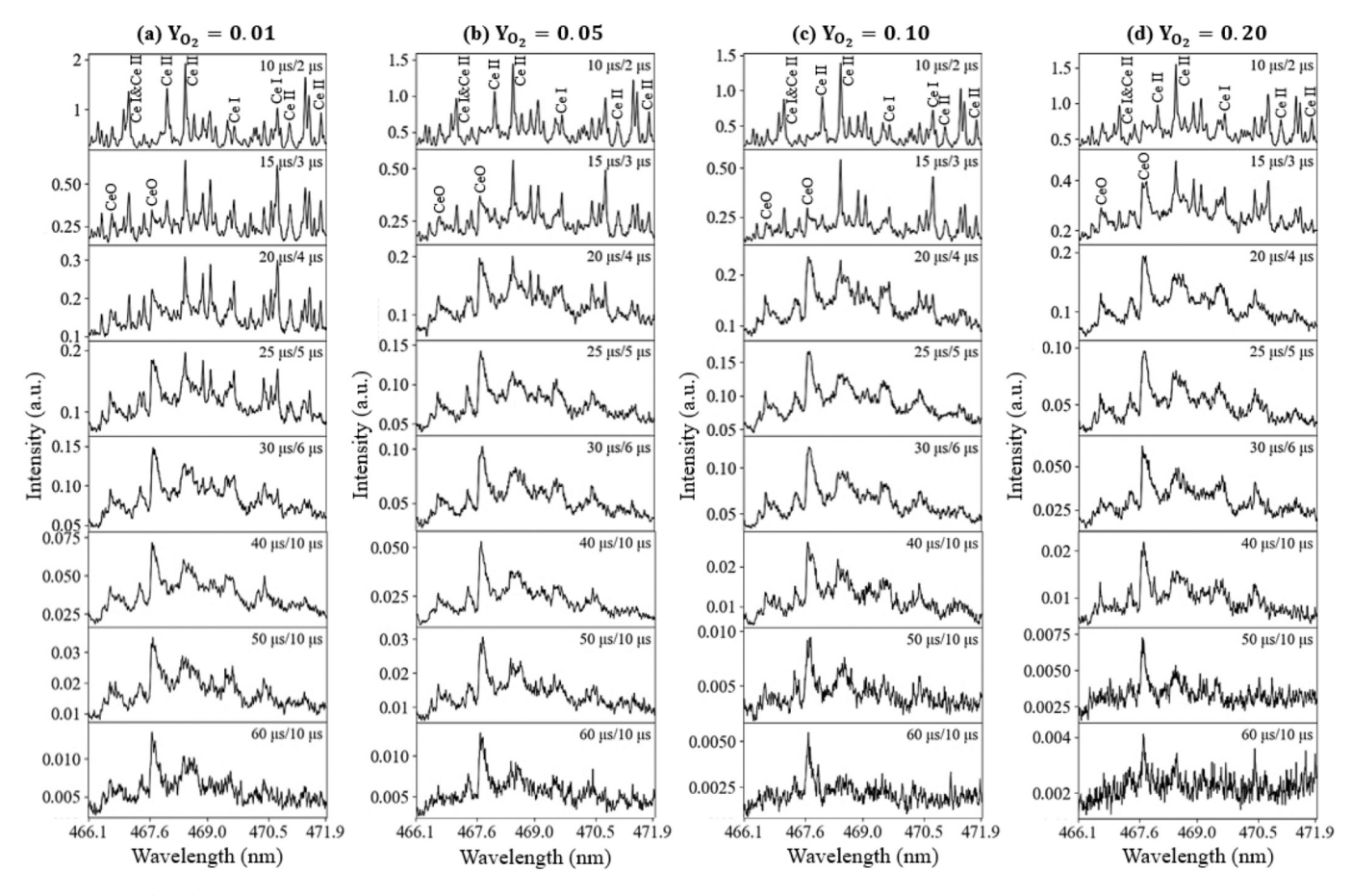


Fig. 3. Temporal evolution of spectroscopic signatures of ns-LA cerium plasmas for the spectral range of 466.1-471.9 nm at 13.3 kPa in argon for oxygen mass fractions of (a) 0.01, (b) 0.05, (c) 0.10, and (d) 0.20. The Q-branch of the CeO  $D_1$ - $X_1$  transitions is situated around 467.7 nm. Times provided represent the delay times and gate widths of the measurements.

overlap significantly with strong atomic emission lines, which makes this molecular feature a great candidate for investigating the oxidation chemistry of Ce LPPs.

The remaining molecular features identified in the spectra include the  $B_2$ - $X_2$  transitions, which also exhibit band heads that do not overlap with strong atomic emission lines yet are characterized by lower intensities than the  $D_1$ - $X_1$  band. Additionally, the vibrational ground state transitions for the  $B_2$ - $X_2$  and  $[14.7]_3$ - $W_2$  bands overlap, although it is believed that the  $B_2$ - $X_2$  band provides a stronger contribution to the sawtooth peak situated around 724.3 nm (see the seventh feature in Fig. 2). Transitions between excited vibrational states, or hot bands, are also observed in the spectrum for the  $D_3$ - $X_3$  and  $B_2$ - $X_2$  transitions. Additional sawtooth peaks beyond those labeled in Fig. 2 are also recognized at 723.7, 727.7, and 727.9 nm. It is believed that these molecular features correspond to CeO, yet to the best of our knowledge these features currently remain unlabeled in the literature.

# 3.2. Effect of oxidation chemistry on the temporal evolution of Ce LPPs

The temporal evolution and persistence of multiple CeO bands was investigated using laser-induced breakdown spectroscopy in an inert argon atmosphere for various mass fractions of oxygen ranging from 0.01 to 0.20. The bulk pressure in the vacuum chamber was maintained around 13.3 kPa, where it has been shown with uranium LPPs that the signal-to-background ratio (SBR) for line emission is maximized at this pressure due to collisional effects without the cooling effect that occurs at higher pressures [71]. Time-resolved emission spectra of cerium for these atmospheric conditions are shown in Figs. 3–5. For all oxygen mass fractions, atomic emission is observed to dominate at early times while

molecular emission becomes predominant at later times. CeO is observed as early as 2  $\mu s$ , yet becomes predominant at earlier times when higher concentrations of oxygen are present. For a spectral range of 466.1–471.9 nm (Fig. 3), at an oxygen mass fraction of ( $Y_{O_2} = 0.01$ ) CeO D<sub>1</sub>-X<sub>1</sub> band is observed to dominant the spectra and obscure any long-lived atomic transitions at times of  $\approx 30 \, \mu s$  and later. For  $Y_{O_2} =$ 0.05, this CeO predominance begins at  $\approx$ 25 us while for higher oxygen mass fractions this occurs at times as early as  $\approx$ 20 µs. This same behavior is observed for the spectral range of 484.2-489.8 nm that encompasses the D<sub>3</sub>-X<sub>3</sub> band (Fig. 4). In contrast, the CeO dominance over the spectral range from 723-735 nm is observed to occur up to 5 µs earlier for all oxygen mass fractions. This may be due to the limited number of atomic transitions that fall within this wavelength range and contribute to the spectrum as compared to the lower wavelengths. The rate of CeO formation and depletion of atomic Ce will be the same across all spectral ranges.

Molecular emission at late times in atmospheres containing low-to-moderate oxygen mass fractions ( $Y_{O_2}=0.01-0.10$ ) is characterized by ro-vibrational signatures that are observable until  $\approx$ 60  $\mu$ s or longer for the Q-branch of the D<sub>1</sub>-X<sub>1</sub> band and the combined peak associated with the R/Q-branch of the B<sub>2</sub>-X<sub>2</sub> band and R-branch of the [14.7]<sub>3</sub>-W<sub>2</sub> band. For these same mass fractions, the emission D<sub>3</sub>-X<sub>3</sub> band is observed to persist for less than 60  $\mu$ s. For oxygen rich environments ( $Y_{O_2}=0.20$ ), the persistence of CeO decreases to  $\approx$ 50  $\mu$ s for all transitions. This behavior is believed to be due to competing reactions that become significant when higher concentrations of oxygen are available to react. Examples of competing reactions include atomic Ce reacting directly with oxygen to form CeO<sub>2</sub>, or CeO reacting with oxygen to form polyatomic oxides. This observed reduction in monoxide persistence for

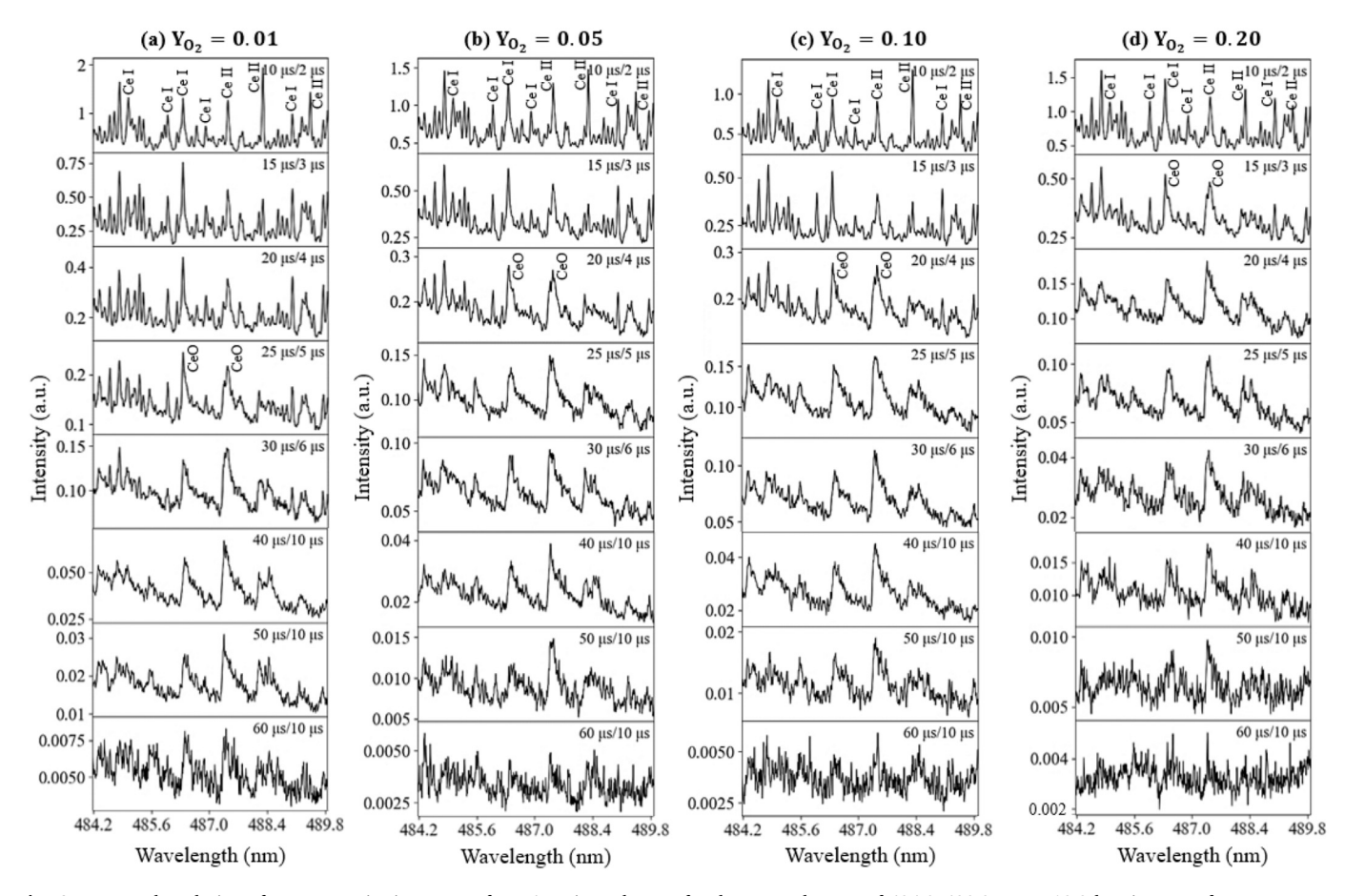


Fig. 4. Temporal evolution of spectroscopic signatures of ns-LA cerium plasmas for the spectral range of 484.2–489.8 nm at 13.3 kPa in argon for oxygen mass fractions of (a) 0.01, (b) 0.05, (c) 0.10, and (d) 0.20. Times provided represent the delay times and gate widths of the measurements.

oxygen rich environments has also been measured with uranium LPPs for UO, and is believed to be due to the formation of polyatomic U<sub>v</sub>O<sub>v</sub> oxides [14,17,21,22]. Thermodynamics and the role of temperature should also be considered as an important factor driving chemical reactions and species lifetimes in the plasma. Chemical reactions are strongly dependent on temperature, where the formation of UO is believed to be favored between  $\approx 3,000-6,000$  K while the formation of higher uranium oxides is believed to occur at lower temperatures [22,24]. Reactive species are also known to influence the temporal evolution of the plasma temperature, such as with U LPPs where a temperature of  $\approx$ 4,000 K was measured at  $\approx$ 20  $\mu$ s for an oxygen partial pressure of 1% as compared ≈1,500 K for 10% O<sub>2</sub> PP at the same delay time [19]. Therefore, due to the lower plasma temperatures polyatomic oxides can form at earlier times when higher concentrations of oxygen are present. To further elucidate this behavior for Ce LPPs, intensities between atomic and molecular transitions over various oxygen concentrations are compared.

Atomic transitions selected for this comparison include Ce II 418.66 nm and Ce I 560.13 nm, which do not overlap significantly with other nearby transitions (see Fig. 6). These transitions are compared to the Q-branch of the CeO  $D_1$ - $X_1$  band, where the branch head does not overlap with other strong atomic and molecular transitions. Integrated intensities are extracted from the measured spectra for these transitions via two separate spectral fitting algorithms. The first method targets atomic transitions, where a custom multivariate optimization algorithm has been developed to fit a Voigt line shape to emission spectra and output the integrated area of that optimized Voigt line shape. Line broadening and intensity contributions due to nearby transitions are included in this analysis. The second algorithm extracts integrated intensities for molecular transitions characterized by triangular or

sawtooth shapes, such as the molecular signatures frequently observed for CeO. This method does not consider contributions due to other nearby and overlapping transitions; therefore, this method should only be applied to strong molecular transitions that do not overlap with other strong molecular transitions. Otherwise, integrated intensities will be overestimated. Additionally, both spectral fitting methods estimate an error associated with the optimized fit to the experimental spectra, which is reflected in uncertainties reported on the intensities.

Normalized integrated intensities are estimated for Ce II 418.66 nm for LIBS measurements performed in argon. These results are shown in Fig. 7 for atmospheres containing different mass fractions of oxygen. The concentration of oxygen in the atmosphere was varied because the associated oxidation chemistry with the cerium plasma is expected to influence the spatiotemporal evolution of atomic cerium species. During the formation of cerium oxides such as CeO, atomic cerium reacts with oxygen and is consumed during this process. This action is reflected in spectroscopic measurements by a faster decay of the atomic signal as the number of unbonded atomic Ce particles is reduced. This behavior is observed in Fig. 7, where the integrated intensities for Ce II decay at a slower rate for oxygen mass fractions of  $Y_{O_2} = 0.05$  and below as compared to argon atmospheres containing higher mass fractions of oxygen. The fastest decay in the Ce II signal is observed for  $Y_{O_2} = 0.10$ while the decay rate is reduced at higher oxygen mass fractions. This indicates that competing reactions do not become significant until a larger quantity, or surplus, of oxygen is available to react.

The formation of CeO in the plasma may also be investigated using ratios between integrated intensities of CeO and atomic Ce species. As the plasma cools, the molecular signal increases in comparison to the atomic signal yielding a ratio of CeO-to-Ce emission that is expected to increase over time. However, it is important to acknowledge that these

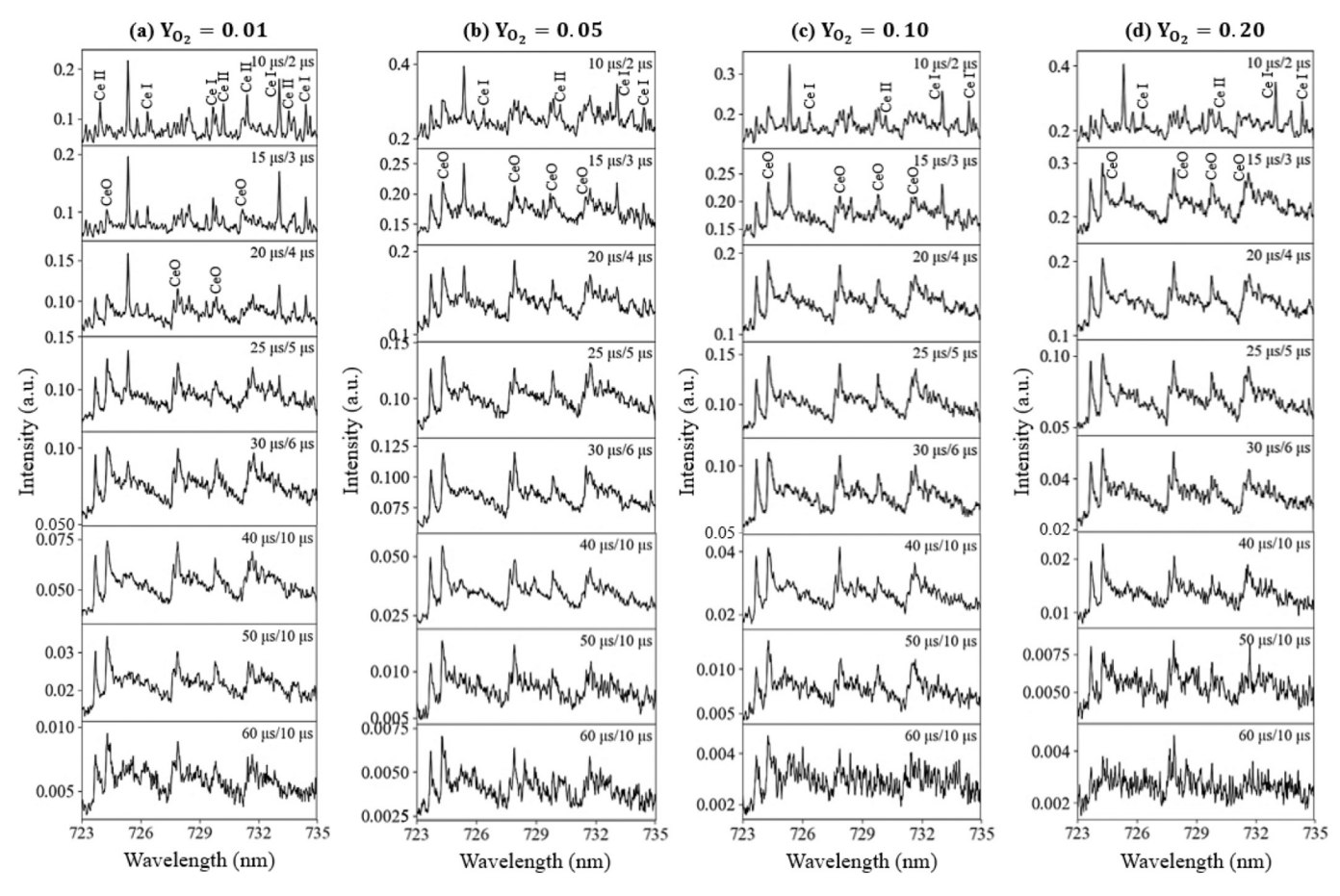
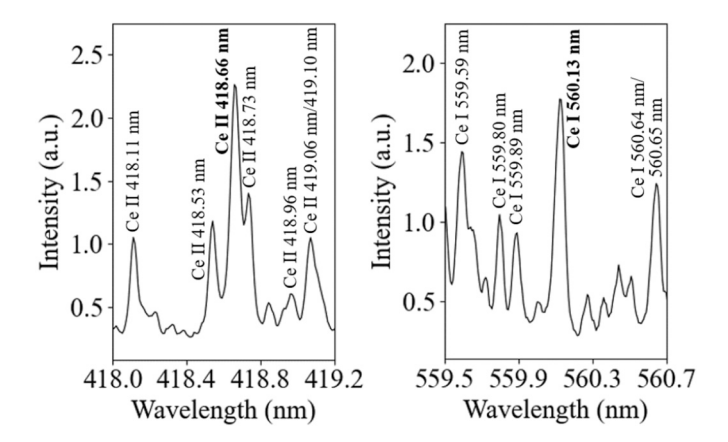
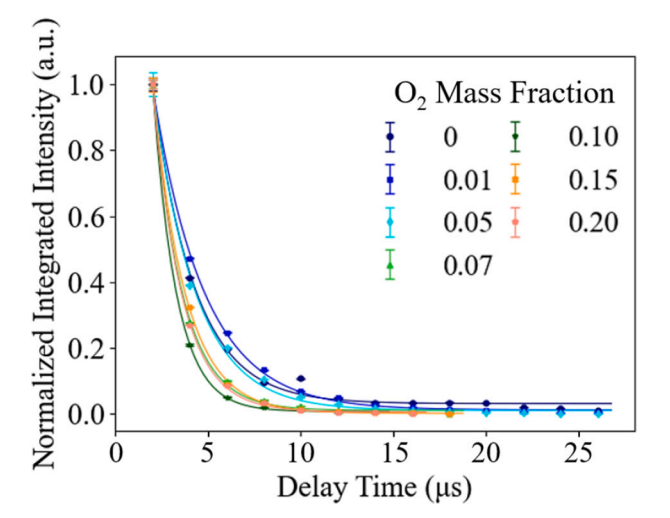


Fig. 5. Temporal evolution of spectroscopic signatures of ns-LA cerium plasmas for the spectral range of 723–735 nm at 13.3 kPa in argon for oxygen mass fractions of (a) 0.01, (b) 0.05, (c) 0.10, and (d) 0.20. Times provided represent the delay times and gate widths of the measurements.



**Fig. 6.** LIBS spectra highlighting the atomic transitions Ce II 418.66 nm and Ce I 560.13 nm used in producing curves on the temporal evolution of the Ce LPP.

ratios will vary based on the atomic and molecular transitions selected to produce them because different transitions decay at different rates. This behavior is evident in Fig. 8, where the values of the ratios and shapes of the curves differ between Ce I and Ce II. Ratios of CeO-to-Ce emission produced using Ce II are consistently larger than those produced using Ce I, which is due to the fact that integrated intensities for Ce I are consistently larger than those for Ce II at later times when the plasma is characterized by lower temperatures. Ratio curves also show that for oxygen mass fractions of 0.05 and below that values tend to be less than those of the other curves, indicating that oxide formation in these



**Fig. 7.** Normalized integrated intensities for Ce II 418.66 nm for various oxygen mass fractions in 13.3 kPa argon. Curves overlaid on the experimental data follow the exponential decay formula. Error bars associated with the data are based on propagated errors associated with the optimization method used to pull out integrated intensities from the spectra as well as the standard deviation on the integrated intensities for repeated measurements.

environments is limited by the availability of oxygen. Conversely, the ratios are maximized at  $Y_{O_2}=0.10$  for Ce II and  $Y_{O_2}=0.15$  for Ce I, suggesting that the rate of formation of CeO is fastest for oxygen mass fractions between 0.10 and 0.15. For higher mass fractions ( $Y_{O_2}=0.20$ ),

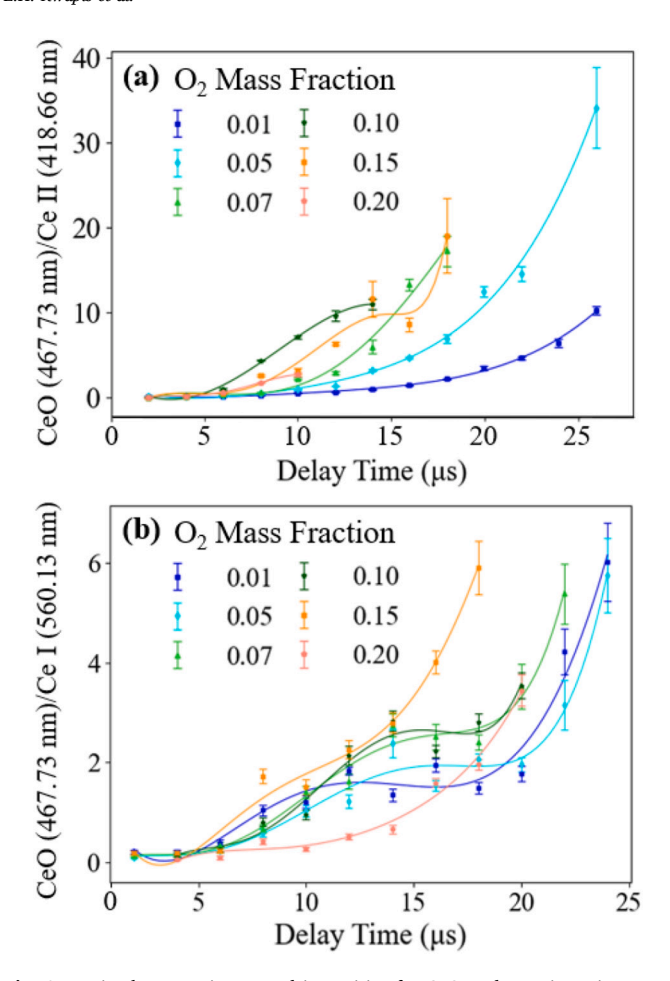


**Fig. 8.** Ratios between integrated intensities for CeO and atomic cerium over various delay times for (a) Ce II 418.66 nm and (b) Ce I 560.13 nm. Curves overlaid on the experimental data are provided for visualization purposes only. Error bars assigned to the ratio values are based on propagated errors associated with the optimization methods used to pull out integrated intensities from the spectra as well as the standard deviation on the integrated intensities for repeated measurements.

the rate of CeO formation and the ratios of CeO-to-Ce emission are decreased, once again suggesting that competing oxidation reactions impact the reactivity of cerium metal plasmas in oxygen rich environments.

#### 3.3. Characteristics of Ce LPPs at atmospheric pressure in air

To study the oxidation behavior of cerium LPPs at atmospheric pressure in air, the process of extracting integrated intensities and estimating ratios between intensities of CeO and atomic cerium transitions is repeated for this atmospheric condition. Results on the temporal evolution for the four atomic transitions (Ce II 413.38 nm, Ce II 418.66 nm, Ce II 428.99 nm, and Ce I 560.13 nm) and the Q-branch of the CeO D<sub>1</sub>-X<sub>1</sub> transition are shown in Fig. 9. It is observed that all Ce II transitions decay at a faster rate than the Ce I transition. Theoretically, this agrees with the Saha equation, which predicts a higher degree of ionization at early times when the plasma is characterized by higher temperatures. This behavior has also been observed for laser-produced plasmas composed of various different elements [72,73]. Furthermore, Ce II 413.38 nm and Ce II 428.99 nm signals are observed to decay at approximately the same rate with an exponential decay constant of  $0.216\pm0.002~\mu s^{-1}$  while the Ce II 418.66 nm signal decays the quickest with a decay constant of 0.240 μs<sup>-1</sup>. This results in lower integrated intensities for the 418.66 nm transition and consequentially yields higher values for the ratios between molecular and atomic emission (see Fig. 9c). Additionally, ratios between the integrated intensities for CeO and Ce I are once again observed to be characterized by lower values than those for the Ce II transitions.

The measured intensities for CeO are observed to peak around  $\approx\!\!15~\mu s$ , after which the monoxide signal decays away at a slower rate than the ionic signal and is characterized by an exponential decay constant of  $0.154~\mu s^{-1}$ . This behavior correlates with the spectroscopic results shown in Fig. 2, where the Q-branch of the  $D_1\text{-}X_1$  CeO transition is clearly identifiable in air at  $15~\mu s$  yet remains obscured by nearby atomic peaks at earlier times.

Lastly, the ratio values for measurements collected in air are directly compared to those measurements collected in argon. It is determined that both cases in air using Ce II 418.66 nm and Ce I 560.13 nm are characterized by approximately the same ratio values as for argon mixed with high concentrations of oxygen ( $Y_{\rm O_2}=0.20$ ), where this mass fraction of oxygen is equivalent to the fraction of oxygen in air. Therefore, the effect of the formation of cerium nitride (CeN) or nitrogen oxides on the oxidation behavior of Ce LPPs in air is negligible.

## 4. Conclusion

Laser-induced breakdown spectroscopy was performed on a cerium metal sample to investigate the spectroscopic signatures and oxidation characteristics of nanosecond laser-induced plutonium surrogate plasmas. Time-resolved spectra of various CeO bands were recorded in the visible spectrum, where the Q-branch of the  $D_1$ - $X_1$  CeO transition was targeted for further analysis of the oxidation behavior of the plasma

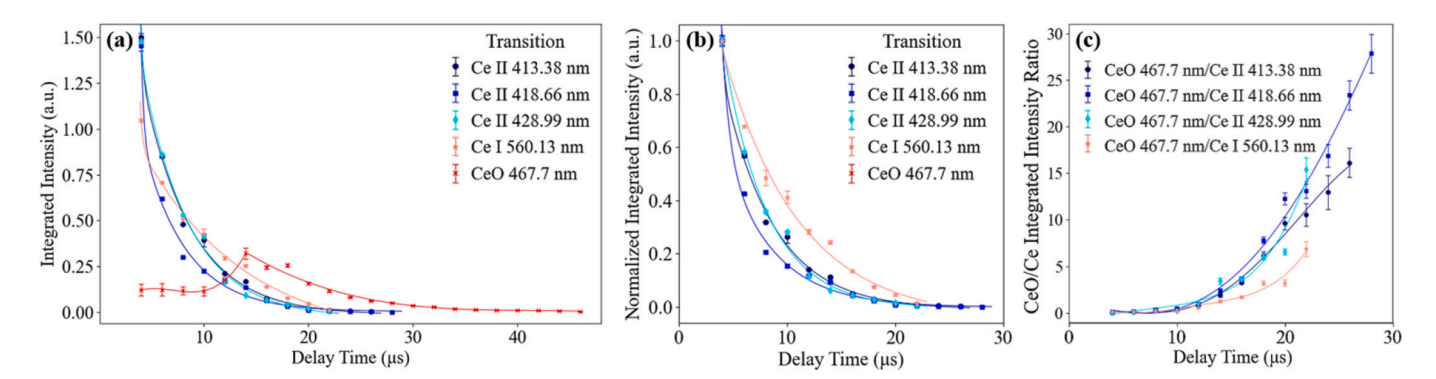


**Fig. 9.** Temporal evolution of atomic cerium and CeO growth at atmospheric pressure in air using (a) integrated intensities, (b) normalized integrated intensities, and (c) ratios between molecular and atomic integrated intensities. Curves overlaid on the experimental data are provided for visualization purposes only. Error bars associated with the data are based on propagated errors associated with the optimization methods used to pull out integrated intensities from the spectra as well as the standard deviation on the integrated intensities for repeated measurements.

due to the isolation of the branch head from any strong atomic transitions. Emission spectra were measured under various atmospheric conditions, including for a reduced-pressure inert argon atmosphere for various concentrations of oxygen as well as at atmospheric pressure in air. Integrated intensities of strong atomic transitions were extracted from the spectra and compared to CeO, where it was observed that the fastest rate of formation of CeO in argon occurred for oxygen mass fractions between 0.10 and 0.15. It is believed that the reduced persistence and growth rate of CeO at higher mass fractions ( $Y_{O_2}=0.20$ ) is due to competing oxidation reactions and lower plasma temperatures. Lastly, the analysis process was repeated for measurements collected at atmospheric pressure in air, and it was determined that the rate of formation of CeO in air is approximately equivalent to the rate of formation in an inert argon environment with an oxygen mass fraction of 0.20.

# CRediT authorship contribution statement

**Emily H. Kwapis:** Conceptualization, Methodology, Software, Validation, Formal-analysis, Investigation, Writing-original-draft, Visualization. **Eliel Villa-Aleman:** Writing-review-editing, Supervision. **Kyle C. Hartig:** Conceptualization, Methodology, Writing-reviewediting, Supervision, Funding-acquisition.

## **Declaration of Competing Interest**

The authors declare that they have no known competing financial interests or personal relationships that could have appeared to influence the work reported in this paper.

#### Data availability

Data will be made available on request.

# Acknowledgements

This document is the result of research funded partially by the University of Florida Herbert Wertheim College of Engineering; Department of Defense Science, Mathematics, and Research for Transformation (SMART) Scholarship-for-Service Program; Department of Energy National Nuclear Security Administration award number DE-NA0003920; National Science Foundation award number CHE1905301; and Defense Threat Reduction Agency award numbers HDTRA1-20–2-0002 and HDTRA1-19–1-0025.

# References

- B. Manard, E. Wylie, S. Willson, Analysis of rare earth elements in uranium using handheld laser-induced breakdown spectroscopy (HH-LIBS), Appl. Spectrosc. 72 (2018) 1653–1660.
- [2] O. Barthélemy, J. Margot, M. Chaker, M. Sabsabi, F. Vidal, T. Johnston, S. Laville, L.B. Drogoff, Influence of the laser parameters on the space and time characteristics of an aluminum laser-induced plasma, Spectrochim. Acta B: At. Spectrosc. 60 (2005) 905–914.
- [3] S. Harilal, C. Bindhu, R. Issac, V. Nampoori, C. Vallabhan, Electron density and temperature measurements of a laser produced carbon plasma, J. Appl. Phys. 82 (1997) 2140–2146.
- [4] K. Muraoka, A. Kono, Topical review: Laser thomson scattering for low-temperature plasmas, J. Phys. D: Appl. Phys. 44 (2011), 043001.
- [5] B. Verhoff, S. Harilal, J. Freeman, P. Diwakar, A. Hassanein, Dynamics of femtoand nanosecond laser ablation plumes investigated using optical emission spectroscopy, J. Appl. Phys. 112 (2012), 093303.
- [6] J. Freeman, S. Harilal, P. Diwakar, B. Verhoff, A. Hassanein, Comparison of optical emission from nanosecond and femtosecond laser produced plasma in atmosphere and vacuum conditions, Spectrochim. Acta B: At. Spectrosc, 87 (2013) 43–50.
- [7] J. Gottfried, Laser-induced plasma chemistry of the explosive RDX with various metallic nanoparticles, Appl. Opt. 51 (2012).
- [8] C. Kimblin, R. Trainham, G. Capelle, R. Russo, X. Mao, LIBS as a surrogate for largescale detonations and means to characterize intermediates, Presented at the FY2014 Site-directed Research and Development (SDRD) Final Review, Las Vegas, NV, United States, Sept. 18, 2014.
- [9] J. Gottfried, Laboratory-scale method for estimating explosive performance from laser-induced shock waves, Propellants Explos. Pyrotech. 40 (2015) 674–681.

- [10] C. Kimblin, R. Trainham, G. Capelle, X. Mao, R. Russo, Characterization of laser-induced plasmas as a complement to high-explosive large-scale detonations, AIP Adv. 7 (2017), 095208.
- [11] P. Skrodzki, N. Shah, N. Taylor, K. Hartig, N. LaHaye, B. Brumfield, I. Jovanovic, M. Phillips, S. Harilal, Significance of ambient conditions in uranium absorption and emission features of laser ablation plasmas, Spectrochim. Acta B: At. Spectrosc. 125 (2016) 112–119.
- [12] K. Hartig, I. Ghebregziabher, I. Jovanovic, Standoff detection of uranium and its isotopes by femtosecond filament laser ablation molecular isotopic spectrometry, Sci. Rep. 7 (2017) 43852.
- [13] D. Weisz, J. Crowhurst, W. Siekhaus, T. Rose, B. Koroglu, H. Radousky, J. Zaug, M. Armstrong, B. Isselhardt, M. Savina, M. Azer, M. Finko, D. Curreli, Formation of <sup>238</sup>U<sup>16</sup>O and <sup>238</sup>U<sup>18</sup>O observed by time-resolved emission spectroscopy subsequent to laser ablation, Appl. Phys. Lett. 111 (2017), 034101.
- [14] E. Kautz, J. Yeak, B. Bernacki, M. Phillips, S. Harilal, Expansion dynamics and chemistry evolution in ultrafast laser filament produced plasmas, Phys. Chem. Chem. Phys. 22 (2020) 8304.
- [15] E. Kautz, M. Phillips, S. Harilal, Unraveling spatio-temporal chemistry evolution in laser ablation plumes and its relation to initial plasma conditions, Anal. Chem. 92 (2020) 13839.
- [16] M. Burton, A. Auner, J. Crowhurst, P. Boone, L. Finney, D. Weisz, B. Koroglu, I. Jovanovic, H. Radousky, K. Knight, The effect of oxygen concentration on the speciation of laser ablation uranium, Sci. Rep. 12 (2022) 4030.
- [17] K. Hartig, S. Harilal, M. Phillips, B. Brumfield, I. Jovanovic, Evolution of uranium monoxide in femtosecond laser-induced uranium plasmas, Opt. Express 25 (2017) 11477
- [18] S. Harilal, B. Brumfield, N. Glumac, M. Phillips, Elucidating uranium monoxide spectral features from a laser-produced plasma, Opt. Express 26 (2018) 20319.
- [19] S. Harilal, E. Kautz, B. Bernacki, M. Phillips, P. Skrodzki, M. Burger, I. Jovanovic, Physical conditions for UO formation in laser-produced uranium plumes, Phys. Chem. Chem. Phys. 21 (2019) 16161.
- [20] E. Kautz, P. Skrodzki, M. Burger, B. Bernacki, I. Jovanovic, M. Phillips, S. Harilal, Time-resolved imaging of atoms and molecules in laser-produced uranium plasmas, J. Anal. At. Spectrom. 34 (2019) 2236.
- [21] P. Skrodzki, M. Burger, I. Jovanovic, M. Phillips, J. Yeak, B. Brumfield, S. Harilal, Plume dynamics and gas-phase molecular formation in transient laser-produced uranium plasmas, Phys. Plasmas 26 (2019), 083508.
- [22] P. Skrodzki, M. Burger, I. Jovanovic, M. Phillips, B. Brumfield, S. Harilal, Tracking of oxide formation in laser-produced uranium plasmas, Opt. Lett. 43 (2018).
- [23] B. Koroglu, J. Crowhurst, M. Armstrong, D. Weisz, J. Zaug, H. Radousky, T. Rose, Speciation measurements using emission and absorption spectroscopy to investigate condensation chemistry for nuclear forensics, Presented at the Methods and Applications of Radioanalytical Chemistry (MARC XI) Conference, Kailua-Kona, HI, United States, April 9–13, 2018.
- [24] B. Koroglu, Z. Dai, M. Finko, M. Armstrong, J. Crowhurst, D. Curreli, D. Weisz, H. Radousky, K. Knight, T. Rose, Experimental investigation of uranium volatility during vapor condensation, Anal. Chem. 92 (2020) 6437–6445.
- [25] E. Weerakkody, D. Weisz, J. Crowhurst, B. Koroglu, H. Radousky, R. Stillwell, J. Jeffries, N. Glumac, Time-resolved formation of uranium and silicon oxides subsequent to the laser ablation of U<sub>3</sub>Si<sub>2</sub>, Spectrochim. Acta B: At. Spectrosc. 170 (2020), 105925.
- [26] E. Weerakkody, N. Glumac, Quantitative absorption spectroscopy of laser-produced plasmas, J. Phys. D: Appl. Phys. 54 (2021), 125201.
- [27] D. Clark, The chemical complexities of plutonium, Los Alamos Sci. 26 (2000) 364–381.
- [28] S. Hecker, Plutonium and its alloys: From atoms to microstructure, Los Alamos Sci. 26 (2000) 290–355.
- [29] J. Blaise, M. Fred, R. Gutmacher, The Atomic Spectrum of Plutonium, Technical Report ANL-83-95, Argonne National Laboratory, Lemont, IL, United States, 1984.
- [30] J. Blaise, M. Fred, R. Gutmacher, Term analysis of the spectrum of neutral plutonium, pu I, J. Opt. Soc. Am. B 3 (1986).
- [31] J. Barefield, E. Judge, J. Berg, S. Willson, L. Le, L. Lopez, Analysis and spectral assignments of mixed actinide oxide samples using laser-induced breakdown spectroscopy (LIBS), Appl. Spectrosc. 67 (2013) 433–440.
- [32] P. Fichet, P. Mauchien, C. Moulin, Determination of impurities in uranium and plutonium dioxides by laser-induced breakdown spectroscopy, Appl. Spectrosc. 53 (1999) 1111–1117.
- [33] C. Smith, M. Martinez, D. Kirk Veirs, D. Cremers, Pu-239/Pu-240 isotope ratios determined using high resolution emission spectroscopy in a laser-induced plasma, Spectrochim. Acta B: At. Spectrosc. 57 (2002) 929–937.
- [34] A. Arko, J. Joyce, L. Morales, J. Terry, R. Schulze, Photoelectron spectroscopy of αand δ-plutonium, Los Alamos Sci. 26 (2000) 168–185.
- [35] M. Butterfield, T. Durakiewicz, E. Guziewicz, J. Joyce, A. Arko, K. Graham, D. Moore, L. Morales, Photoemission of surface oxides and hydrides of delta plutonium, Surf. Sci. 571 (2004) 74–82.
- [36] S. Harilal, C. Murzyn, E. Kautz, M. Edwards, S. Sinkov, S. Bisson, S. Mitra, J. Martin, Spectral dynamics and gas-phase oxidation of laser-produced plutonium plasmas, J. Anal. At. Spectrom. 36 (2021).
- [37] L. Kaledin, M. Heaven, Electronic spectroscopy of UO, J. Mol. Spectrosc. 185 (1997) 1–7.
- [38] L. Kaledin, J. McCord, M. Heaven, Laser spectroscopy of UO: Characterization and assignment of states in the 0- to 3-ev range, with a comparison to the electronic structure of ThO, J. Mol. Spectrosc. 164 (1994).
- [39] M. Heaven, J. Nicolai, S. Riley, E. Parks, Rotationally resolved electronic spectra for uranium monoxide, Chem. Phys. Lett. 119 (1985).

- [40] R. Barrow, R. Clements, S. Harris, P. Jenson, The electronic spectrum of gaseous GeO, Astrophys. J. 229 (1979).
- [41] L. Kaledin, J. McCord, M. Heaven, Laser spectroscopy of CeO: Characterization and assignment of states in the 0–3 ev range, J. Mol. Spectrosc. 158 (1993) 40–61.
- [42] C. Linton, M. Dulick, R. Field, P. Carette, P. Leyland, R. Barrow, Electronic states of the CeO molecule: Absorption, emission, and laser spectroscopy, J. Mol. Spectrosc. 102 (1983) 441–497.
- [43] C. Linton, J. Chen, T. Steimle, Permanent electric dipole moment of cerium monoxide, J. Phys. Chem. A 113 (2009) 13379–13382.
- [44] C. Linton, M. Dulick, R. Field, Laser spectroscopy of CeO: Fluorescence of the C<sub>1</sub>-X<sub>1</sub> and D<sub>3</sub>-X<sub>3</sub> systems, J. Mol. Spectrosc. 78 (1979).
- [45] M. Moore, Y. Tao, Aerosol Physics Considerations for using Cerium Oxide CeO<sub>2</sub> as a Surrogate for Plutonium Oxide PuO<sub>2</sub> in Airborne Release Fraction Measurements for Storage Container Investigations, Technical Report LA-UR-17-21241, Los Alamos National Laboratory, Los Alamos, NM, United States, 2017.
- [46] Y. Park, T. Taylor, A. Atencio, D. Butt, Kinetics of and Atmospheric Effects on Gallium Removal from a CeO<sub>2</sub> Based Mixed Oxide Surrogate, Technical Report LA-UR-98-2735, Los Alamos National Laboratory, Los Alamos, NM, United States, 1999
- [47] R. Hoyt, Thermal Property Evaluation of Cerium Dioxide and Cerium Dioxide-Magnesium Oxide: Powders for Testing Plutonium Stabilization Furnaces, Technical Report HNF-11207, Fluor Hanford, Richland, WA, United States, 2002.
- [48] J. Marra, A. Cozzi, R. Pierce, J. Pareizs, A. Jurgensen, D. Missimer, Cerium as a Surrogate in the Plutonium Immobilized Form, Technical Report WSRC-MS-2001-00007, Westinghouse Savannah River Company, Aiken, SC, United States, 2001.
- [49] D. Kolman, Y. Park, M. Stan, R. Hanrahan Jr., D. Butt, An Assessment of the Validity of Cerium Oxide as a Surrogate for Plutonium Oxide Gallium Removal Studies, Technical Report LA-UR-99-491, Los Alamos National Laboratory, Los Alamos, NM, United States, 1999.
- [50] H. Zheng, F. Yueh, T. Miller, J. Singh, K. Zeigler, J. Marra, Analysis of plutonium oxide surrogate residue using laser-induced breakdown spectroscopy, Spectrochim. Acta B: At. Spectrosc. 63 (2008) 968–974.
- [51] K. Suzuki, M. Kato, T. Sunaoshi, H. Uno, U. Carvajal Nunez, A. Nelson, K. McClellan, Thermal and Mechanical Properties of CeO<sub>2</sub>, Technical Report LA-UR-18-23161, Los Alamos National Laboratory, Los Alamos, NM, United States, 2018.
- [52] J. Haschke, T. Allen, L. Morales, Surface and corrosion chemistry of plutonium, Los Alamos Sci. 26 (2000) 252–273.
- [53] L. Dinh, J. Stanford, C. Saw, A. Nelson, R. Gollott, J. Haschke, P. Allen, C. Gardner, C. Hrousis, W. Siekhaus, W. McLean, Spectroscopic ellipsometry extraction of optical constants for materials from oxide covered samples: Application to the plutonium/oxides system, J. Appl. Phys. 125 (2019), 183102.
  [54] D. Wheeler, Kinetics and mechanism of the oxidation of certum in air at ambient.
- temperature, Corros. Sci. 111 (2016) 52–60.
- [55] D. Mullins, The surface chemistry of cerium oxide, Surf. Sci. Rep. 70 (2015) 42–85.
- [56] A. Panda, A. Singh, M. Mishra, R. Thirumurugesan, P. Kuppusami, E. Mohandas, Plasma plume behavior of laser ablated cerium oxide: Effect of oxygen partial pressure, Laser Part. Beams 32 (2014) 429–435.

- [57] M. Onbasli, T. Goto, X. Sun, N. Huynh, Integration of bulk-quality thin film magneto-optical cerium-doped yttrium iron garnet on silicon nitride photonic substrates, Opt. Express 22 (2014) 25183.
- [58] M. Engholm, P. Jelger, F. Laurell, L. Norin, Improved photodarkening resistivity in ytterbium-doped fiber lasers by cerium codoping, Opt. Lett. 34 (2009) 1285.
- [59] M. Miyabe, M. Oba, H. Iimura, K. Akaoka, Y. Maruyama, I. Wakaida, Spectroscopy of laser-produced cerium plasma for remote isotope analysis of nuclear fuel, Appl. Phys. A 101 (2010) 65–70.
- [60] M. Martin, S. Allman, D. Brice, R. Martin, N. Andre, Exploring laser-induced breakdown spectroscopy for nuclear materials analysis and in-situ applications, Spectrochim. Acta B: At. Spectrosc. 74–75 (2012) 177–183.
- [61] A. Williams, K. Bryce, S. Phongikaroon, Measurement of cerium and gadolinium in solid lithium chloride-potassium chloride salt using laser-induced breakdown spectroscopy (LIBS), Appl. Spectrosc. 71 (2017) 2302–2312.
- [62] A. Williams, S. Phongikaroon, Elemental detection of cerium and gadolinium in aqueous aerosol using laser-induced breakdown spectroscopy, Appl. Spectrosc. 70 (2016) 1700–1708.
- [63] K. Campbell, E. Judge, J. Barefield II, J. Colgan, D. Kilcrease, K. Czerwinski, S. Clegg, Laser-induced breakdown spectroscopy of light water reactor simulated used nuclear fuel: main oxide phase, Spectrochim. Acta B: At. Spectrosc. 133 (2017) 26-23.
- [64] D. Choi, Y. Gong, H. Kim, B. Gwak, Y. Lee, B. Han, H. Shin, Remote detection of cerium using laser-induced breakdown spectroscopy, in: Proc. of the 2013 Conf. on Lasers and Electro-optics Pacific Rim (CLEO-PR), 2013. doi:10.1109/ CLEOPR.2013.6600572.
- [65] R. Kurucz, B. Bell, Atomic line data kurucz CD-ROM No. 23, 1995.
- [66] Z. Li, H. Lundberg, G. Wahlgren, C. Sikström, Lifetime measurements of Ce I, Ce II, and Ce III using time-resolved laser spectroscopy with application to stellar abundance determinations of cerium, Phys. Rev. A 62 (2000), 032505.
- [67] W. Martin, Low energy levels of neutral cerium (Ce I), J. Opt. Soc. Am. 53 (1963) 1047–1050.
- [68] W. Martin, R. Zalubas, L. Hagan, Atomic energy levels The rare-earth elements, Nat. Stand. Ref. Data Ser. (1978) Nat. Bur. Stand. (U.S.), NSRDS–NBS 60.
- [69] D. Nitz, J. Curry, M. Buuck, A. DeMann, N. Mitchell, W. Shull, Transition probabilities of Ce I obtained from boltzmann analysis of visible and near-infrared emission spectra, J. Phys. B: At. Mol. Opt. Phys. 51 (2018), 045007.
- [70] C. Corliss, Wavelengths and energy levels of the second spectrum of cerium (Ce II), J. Res. Natl. Bur. Stand. A Phys. Chem. 77A (1973) 419–546.
- [71] N. LaHaye, S. Harilal, P. Diwakar, A. Hassanein, Persistence of uranium emission in laser-produced plasmas, J. Appl. Phys. 115 (2014), 163301.
- [72] M. Oujja, J. Camacho, D. Paradela, M. Castillejo, R. de Nalda, Emission characteristics and dynamics of neutral, ionic and molecular species in a laser produced CaF<sub>2</sub> plasma, J. Ouant. Spectrosc. Radiat. Transfer 276 (2021), 107924.
- [73] M. Singh, A. Sarkar, Time-resolved evaluation of uranium plasma in different atmospheres by laser-induced breakdown spectroscopy, Plasma Sci. Technol. 20 (2018), 125501.